Implementation of synthetic fast-ion loss detector and imaging heavy ion beam probe diagnostics in the 3D hybrid kinetic-MHD code MEGA

(iD) **P. Oyola**, (iD) **J. Gonzalez-Martin**, (iD) **M. Garcia-Munoz, et al.**

COLLECTIONS

Paper published as part of the special topic on Proceedings of the 23rd Topical Conference on High-Temperature Plasma Diagnostics

View Online   Export Citation   CrossMark

ARTICLES YOU MAY BE INTERESTED IN

Design and simulation of an imaging neutral particle analyzer for the ASDEX Upgrade tokamak
Review of Scientific Instruments **92**, 043554 (2021); https://doi.org/10.1063/5.0043768
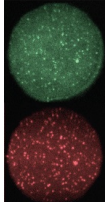
Mechanisms of energetic-particle transport in magnetically confined plasmas
Physics of Plasmas **27**, 030901 (2020); https://doi.org/10.1063/1.5136237

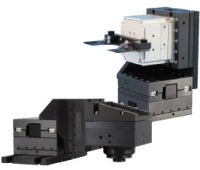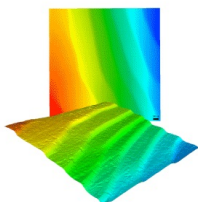Upgrade and absolute calibration of the JET scintillator-based fast-ion loss detector
Review of Scientific Instruments **92**, 043553 (2021); https://doi.org/10.1063/5.0043760

Nanopositioning Systems

Modular Motion Control

AFM and NSOM Instruments

Single Molecule Microscopes

MCL MAD CITY LABS INC.
www.madcitylabs.com

Implementation of synthetic fast-ion loss detector and imaging heavy ion beam probe diagnostics in the 3D hybrid kinetic-MHD code MEGA

P. Oyola,[1,a] J. Gonzalez-Martin,[2,3] M. Garcia-Munoz,[1,2] J. Galdon-Quiroga,[4] G. Birkenmeier,[4,5]
E. Viezzer,[1,2] J. Dominguez-Palacios,[1,2] J. Rueda-Rueda,[1] J. F. Rivero-Rodriguez,[2,3] Y. Todo,[6]
and ASDEX Upgrade Team[b]

AFFILIATIONS

[1] Department of Atomic, Molecular and Nuclear Physics, Universidad de Sevilla, Sevilla 41012, Spain
[2] Centro Nacional de Aceleradores (CNA) CSIC, 41092 Sevilla, Spain
[3] Department of Mechanical Engineering and Manufacturing, Universidad de Sevilla, Sevilla 41092, Spain
[4] Max Planck Institute for Plasma Physics, 85748 Garching, Germany
[5] Physics Department E28, Technical University Munich, 85748 Garching, Germany
[6] National Institute for Fusion Science, 509-5292 Toki, Japan

Note: Paper published as part of the Special Topic on Proceedings of the 23rd Topical Conference
on High-Temperature Plasma Diagnostics.
a) Author to whom correspondence should be addressed: poyola@us.es
b) See author list of Meyer et al. Nucl. Fusion 59, 112014 (2019).

ABSTRACT

A synthetic fast-ion loss (FIL) detector and an imaging Heavy Ion Beam Probe (i-HIBP) have been implemented in the 3D hybrid kinetic-magnetohydrodynamic code MEGA. First synthetic measurements from these two diagnostics have been obtained for neutral beam injection-driven Alfvén Eigenmode (AE) simulated with MEGA. The synthetic FILs show a strong correlation with the AE amplitude. This correlation is observed in the phase-space, represented in coordinates (P_ϕ, E), being toroidal canonical momentum and energy, respectively. FILs and the energy exchange diagrams of the confined population are connected with lines of constant E', a linear combination of E and P_ϕ. First i-HIBP synthetic signals also have been computed for the simulated AE, showing displacements in the strike line of the order of ~1 mm, above the expected resolution in the i-HIBP scintillator of ~ 100 μm.

Published under license by AIP Publishing. https://doi.org/10.1063/5.0043757

I. INTRODUCTION

In magnetically confined fusion plasmas, Alfvén Eigenmodes (AEs) can be excited by various fast-ion sources, such as neutral beam injection (NBI) and fusion-born alpha particles. In turn, AEs can enhance the fast-ion transport and can lead to fast-ion losses (FILs) toward the first wall in fusion devices, resulting in hazardous heat loads in future reactors, such as ITER.[1,2]

Previous work has been carried out to characterize AEs experimentally,[3–5] focused on the identification of the fast-ion transport induced by these modes and the poloidal structures of the modes. In the ASDEX Upgrade (AUG) tokamak, the poloidal array of the

fast-ion loss detectors[6–8] (FILDs) has detected that the fast-ion losses are correlated with the AE amplitude and frequency, demonstrating the AE and fast-ion interaction. Accurate characterization of these losses and the mode structures plays a key role in understanding the fast-ion confinement.[9–12]

In this work, these experiments are modeled with the 3D non-linear hybrid kinetic-magnetohydrodynamic (MHD) code MEGA.[13] Two synthetic diagnostics have been developed in MEGA, providing further insight into the Alfvénic activity, by studying two fundamental key points: the fast-ion loss and the radial structures.

These synthetic diagnostics are based on two of the diagnostic systems in AUG: the poloidal array of the Fast-Ion Loss

Detector (FILD) and the imaging Heavy-Ion Beam Probe[14–16] (i-HIBP). For the former, a realistic 3D wall for the AUG tokamak has been implemented in MEGA showing a correlation between the fast-ion losses toward the wall and the AE activity in the simulations. For the latter, a predictive study of the synthetic signal demonstrates the capability of the i-HIBP for measuring an AE located in the midradius.

This paper is organized as follows: The model implemented in the code MEGA is briefly described in Sec. II where the implementation of the realistic 3D wall is described. The implementation of the synthetic diagnostic for the i-HIBP is described in Sec. III. Section IV is devoted to the analysis of MEGA simulations showing the fast-ion losses and the synthetic signal for the i-HIBP diagnostic. A summary is given in Sec. V.

II. MEGA AND THE REALISTIC 3D WALL

MEGA is a numerical code that computes the self-consistent evolution of a bulk plasma and the fast-ion population in realistic 3D configurations using cylindrical coordinates. In this code, the bulk plasma is modeled using the complete non-linear single-fluid resistive-MHD equations.[13,17] Coupling between bulk plasma and fast-ion population is done via the current density in the momentum balance equation.

The set of MHD equations is spatially discretized using fourth order finite differences on a cylindrical grid, covering the full tokamak geometry. The fast-ion distribution is sampled by markers covering the 5D reduced phase-space $(X, p_\parallel, \mu)$, with X being the guiding-center position, $p_\parallel$ being the parallel momentum, and μ being the magnetic dipole moment. These markers are evolved using the gyro-kinetic equations with Finite Larmor Radius (FLR) corrections. The fast-ion distribution is evolved using *particle-in-cell* with the δf method.[18]

The cylindrical grid resolution has been chosen to be $(N_R, N_\phi, N_z) = (128, 64, 256)$. Toroidal mode numbers with $n > 5$ are filtered out. The time evolution is obtained using an explicit fourth order Runge–Kutta scheme.

Experimental profiles and magnetic reconstructions from AUG pulse #34 570 are used as inputs for the MEGA simulations. The corresponding profiles are shown in Fig. 1. The initial fast-ion distribution is given by a modeled off-axis NBI slowing-down distribution using a Gaussian term[8] for the spatial dependence. The initial

distribution function used in this work is

$$F_{\text{phase-space}} \propto e^{-\frac{(\rho-\rho_0)^2}{2(\Delta\rho)^2}} \frac{1}{v^3 + v_{\text{crit}}^3} \text{erfc}\left(\frac{v - v_{\text{birth}}}{\Delta v}\right) e^{-\frac{(\Lambda-\Lambda_0)^2}{2(\Delta\Lambda_0)^2}}, \quad (1)$$

where ρ is the normalized poloidal magnetic flux. Spatial parameters have been fixed to $\rho_0 = 0.4$ and $\Delta\rho = 0.15$ in this work. v_{birth} is the birth velocity and has been set to 93 keV, and $\Delta v = 0.05 \cdot v_{\text{birth}}$. For the pitch-angle, a Gaussian dependence in $\Lambda \equiv 1 - \lambda^2 = \frac{\mu B}{E}$ is introduced. The pitch-angle parameters have been set to $\Lambda_0 = 0.55$ and $\Delta\Lambda_0 = 0.20$ in this work. Finally, v_{crit} is the critical velocity.[19]

The parameter regulating the fast-ion density, $\beta_{\text{fi}} = \frac{p_{\text{fi}}}{B_{\text{axis}}^2/2\mu_0}$, is set to $\beta_{\text{fi}} = 0.67\%$, with p_{fi} being the fast-ion pressure. This value corresponds to the NBI6 for the same discharge. Note that this work does not intend to reproduce the Toroidal Alfvén Eigenmodes (TAEs) observed in the experiment but to provide a suitable simulation case to test the newly implemented synthetic diagnostics. A detailed comparison to the experiment is ongoing.[20]

A 3D wall has been implemented in MEGA, allowing us to stop the evolution of fast-ion markers when they reach the first wall. The mapping of the wall to the cylindrical grid (where the MHD equations are solved) allows for a fast implementation of the 3D wall, without a significant impact on the simulation efficiency (less than 1%). In Fig. 2, a poloidal cut of the mapped wall in MEGA is shown. The regions marked in yellow (some of them lie behind the 2D wall model represented by the thicker black lines) determine where the fast-ion evolution will be stopped and considered as fast-ion losses (FILs).

III. SYNTHETIC i-HIBP DIAGNOSTIC

The i-HIBP diagnostic injects a heavy-neutral primary beam (^{133}Cs or ^{85,87}Rb) into the plasma that ionizes due to multiple processes. These ionized particles, forming the secondary beam, start
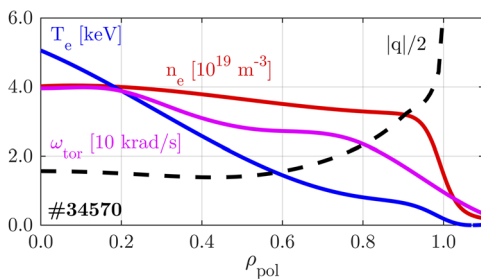

FIG. 1. Density, temperature, and toroidal rotation used as starting points for MEGA simulations, taken from the AUG tokamak discharge #. 34 570 ($t = 3.53$ s). The reconstructed q-profile is shown in dashed lines.
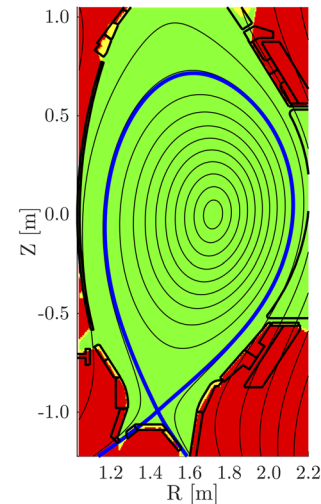

FIG. 2. Map of the wall (here represented for $\phi = 0°$) used in MEGA to obtain the fast-ion losses. Green and red regions indicate inside/outside simulation domains for the FI markers. The first wall is used as a limit where fast-ion markers are captured. Solid lines represent flux surfaces. The separatrix is indicated in blue.

a gyromotion until reaching a scintillator plate. The signal on the scintillator translates into a twofold information: the intensity of the strike line provides the plasma density (n_e); and the strike line position and shape provide information on the magnetic and electric fields, $\boldsymbol{B}$ and $\boldsymbol{E}$, respectively.[16]

The synthetic diagnostic of the i-HIBP, the new *i-HIBPsim* code, is based on kinetic simulations for the two main species, the heavy-neutrals (primary beam) and heavy-ions (secondary beam). Markers are launched at the injection port and tracked into the plasma using a Boris leap-frog scheme.[21] In this work, an infinitely small beam is used, i.e., the width of the beam and divergences are set to zero. The secondary beam birth distribution is obtained by using a beam attenuation model, $\dot{W}_j = -\sum_{k \in \text{reactions}} W_j n_k \langle \sigma v \rangle_k$, where the sum is over all possible reactions that attenuate the beam, n_k is the secondary reactant density, and $\langle \sigma v \rangle_k$ is the reaction rate of the kth reaction. Only two reactions are considered to generate the attenuation of the primary: the electron-impact ionization[22] and the charge-exchange reactions with main-ions.[23–25] The single-ionization step is implemented in the simulation code as the recombination via charge-exchange (i.e., $Cs^+ + D^0 \rightarrow Cs^0 + D^+$) is expected to be much smaller, since the neutral density in AUG is of the order[26] of $n_0 \sim 10^{16} \, \text{m}^{-3}$. Impurity-induced ionization reaction rates, as extrapolated from lithium in Ref. 27, are negligible compared to the main ion charge-exchange and electron-impact ionization rates. This, combined with the typical impurity concentration ($\sim 1\%$ after the boronization[28]), makes this interaction negligible, compared to collisions with electrons and main ions.

The secondary beam will travel following gyro-orbits until hitting the scintillator, determined via a ray-triangle algorithm.[29] The beam-attenuation equation is also used to determine the secondary beam flux into the scintillator. A single-step ionization is used for the secondary beam considering only the electron-impact ionization.[30,31] Charge-exchange recombination for the secondary beam is not taken into account, as for the primary beam.

Markers evolve in a fully 3D input electromagnetic field, allowing for a direct connection with MEGA. The electromagnetic perturbations computed by MEGA for a certain plasma phenomenon can be used to feed the synthetic diagnostic and obtain the predicted signal.

In previous experiments in fusion devices, such as TJ-II, a similar diagnostic, the HIBP, has been used to detect and characterize the poloidal mode numbers and structure of the AE.[32] The scintillator-based i-HIBP will provide the high spatial resolution measurements, as shown in Fig. 5 (up to 100 μm in the scintillator).

IV. SIMULATION RESULTS

The off-axis fast-ion distribution produces in the plasma a TAE located at the midradius ($\rho_{\text{pol}} = 0.70$). This example case, using the realistic 3D wall, already suggests an important fast-ion loss mechanism via the wave-particle resonances. The location of the AE, as shown in Fig. 3(b), is close enough to the edge for the heavy-ions in the i-HIBP to feel the perturbations. The green lines represent trajectories for ^{85}Rb under the perturbed magnetic field, proving the possible range of detection.
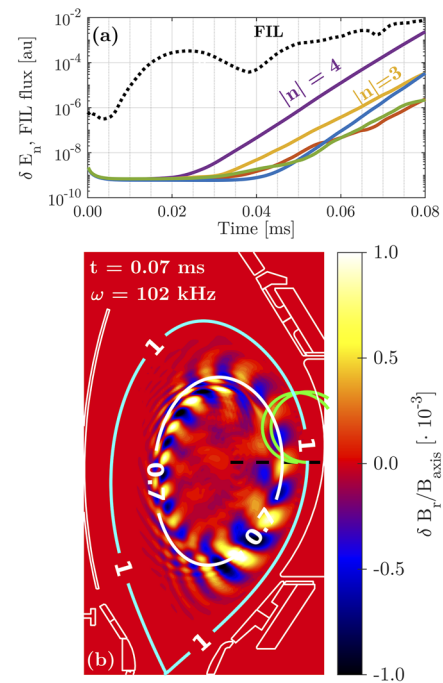

FIG. 3. (a) Solid lines denote the evolution of the energy associated with the toroidal $|n|$ mode numbers. Dashed lines represent the FIL flux associated with the region in velocity space $\mu \in (3.0, 5.0) \cdot 10^{-15}$ J/T. (b) Poloidal representation of the perturbation at $t = 0.07$ ms. Flux surfaces corresponding to $\rho_{\text{pol}} = 0.70$ and 1.00 as well as the 2D wall structures are represented for visual guidance. ^{85}Rb orbits obtained with *i-HIBPsim* and discussed in Sec. IV B are represented in green.

The implementation of an off-axis initial fast-ion spatial distribution leads to Alfvénic activity closer to the plasma edge. In Fig. 3(a), the toroidal mode energy in the bulk plasma is shown on a logarithmic scale. The $|n| = 4$ mode shows the largest growth and dominates the plasma phenomena. The fast-ion *flux* for a given $\mu \in (3.0, 5.0) \cdot 10^{-15}$ J/T interval is represented by dashed lines. Note that to avoid the inclusion of unrealistic fast-ion prompt losses in the simulation, the quantity $|\delta w_j| N_j$ has been presented instead, where $|\delta w_j|$ is the differential weight evolution with respect to the equilibrium and N_j is the number of particles represented initially by the marker. The markers strongly interacting with the mode have a higher $|\delta w_j|$, hence allowing us to focus on fast-ion loss induced by the mode.

In Fig. 3(b), the poloidal structure of the mode at $t = 0.07$ ms is shown. The mode is located around the surface $\rho_{\text{pol}} = 0.7$, superimposed for visual guidance. A Fourier transform of its time evolution shows that the frequency of the mode is $f = 102$ kHz.

A. Synthetic fast-ion losses

In the AUG tokamak, strong TAE-coherent fast-ion losses have been detected with the FILD array.[11] The induced losses can be explained by the magnetic perturbation producing an open trajectory, without a net energy exchange, or via a power exchange with the mode resulting in an orbit kick away from the confined region.

Fast-ion losses in MEGA simulations have been obtained using a self-consistent approach, capturing the fast-ion markers during the simulations. To identify whether these losses are produced by a significant interaction with the AE, the phase-space is represented by variables $\left(P_\phi, E, \mu\right)$ being toroidal canonical momentum, energy, and magnetic moment, respectively. In Figs. 4(a) and 4(b), the phase-space for $\mu \in (3.0, 5.0) \cdot 10^{-15}$ J/T is shown. For the confined population, (a) the instantaneous energy exchange is presented, indicating the region where the mode interacts the strongest with the fast-ions. For the FIL, (b) the impinging flux onto the 3D wall is presented.

In the presence of a wave with a given low and constant frequency, ω_n, and toroidal mode number n, the conserved quantity[4] is $E' = E - \frac{\omega_n}{n} P_\phi$. Contour lines with this quantity are superimposed in Figs. 4(a) and 4(b). Fast-ions that drive the AE drift away and hit the wall following constant E' lines. As a visual guidance, the divertor region is represented in both figures as a cyan dashed line, which is the region with the largest heat loads. In Fig. 4(c), the FIL flux is represented in the angular plane only below the midplane ($\theta = 0$), since it is the region receiving most of the FIL flux.

A simulation with only the toroidal mode numbers $|n| = 0, 4$, i.e., filtering the rest of the Fourier components, shows that both the
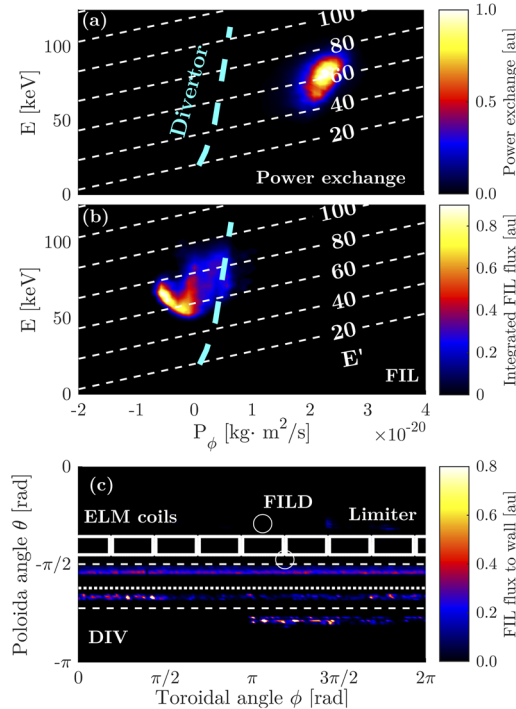
confined population energy exchange are still present in the same location. The FILs in these simulations do not differ significantly from the multi-n simulation. We can conclude that the fast-ion transport and losses are dominated by their interaction with the toroidal mode number $n = 4$.

This analysis suggests that the fast-ion losses are predominately expulsed from the plasma due to the energy exchange with the AE during the linear growth phase. This would play a central role in the interpretation of the FILD experiments in the AUG tokamak, since it connects the fast-ion loss measurements to an energy exchange with the mode.

B. Synthetic i-HIBP signal

The simulated AE is used here to construct the i-HIBP synthetic signal. The total mode amplitude is of the order of $\delta B_r / B_{\rm axis} \sim 10^{-3}$, typical from NBI-driven AE experiments in the AUG tokamak, allowing us to obtain realistic estimates of the i-HIBP signal.

The signal on the scintillator has been obtained by tracking both the primary and secondary beams using the *i-HIBPsim* synthetic diagnostic, described in Sec. III. The long gyro-radius (of the order of 20 cm in the current setup, with $E = 70$ keV for ^{85,87}Rb, $E = 50$ keV for ^{133}Cs, and $B = 2.5$ T) of the heavy-ion takes them further within the plasma where electromagnetic perturbations modify their orbits before reaching the scintillator. In Fig. 5, the strike line on the scintillator for ^{87}Rb is shown for the baseline scenario, i.e., without perturbations. For visual guidance, points with the birth $\rho_{\rm pol}$ location are superimposed, and the sign convention for the line perturbation is presented.

Simulations with and without the AE perturbations have been carried out in order to assess the changes in the strike line on the scintillator. The perturbation case has been analyzed with and without the generated AE electric field ($\delta E_r \sim 6$ kV/m) in order to isolate
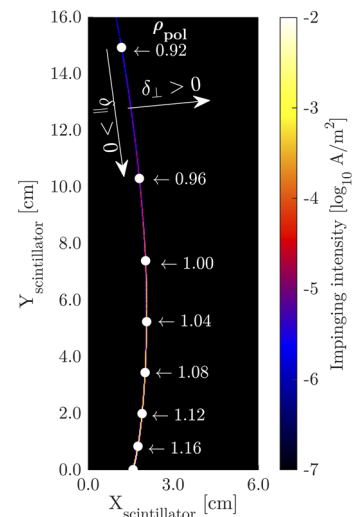

FIG. 4. (a) and (b) Slice of the velocity space for the fast-ion, corresponding to $\mu \in (3.0, 5.0) \cdot 10^{-15}$ J/T. (a) Instantaneous power exchange of the confined fast-ion population at $t = 0.059$ ms, superimposed with the lines of constant E'. Dashed blue lines represent the divertor surface projected on the velocity space. (b) Fast-ion loss flux (number of fast-ions hitting the wall) for times $t > 0.060$ ms. (c) Toroidal plane of the fast-ion losses $t > 0.060$ ms, where important structures are represented. Here, $\theta = 0$ represents the midplane and $\theta = -\pi$ denotes the lower divertor.

FIG. 5. Strike line representation for the equilibrium case for the ^{87}Rb case. The origin points of the secondary are displayed in white dots. The convention for strike line perturbations is defined in this figure: perpendicular to the strike line (mostly in the X-direction) is positive to the right.
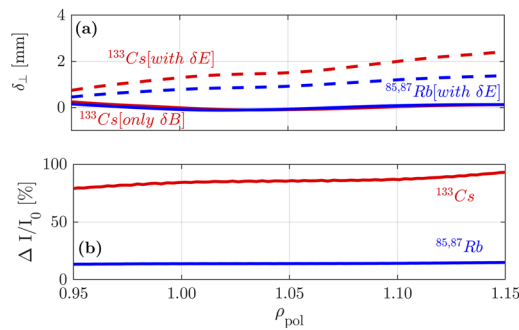
FIG. 6. Impact on the strike line of the simulated TAE. (a) Perpendicular displacement (with respect to the one defined in Fig. 5) of the strike line due to magnetic perturbation alone (solid lines) and including both electric and magnetic perturbations (dashed lines). (b) Relative deviation in the intensity seen in the strike line with respect to the equilibrium. Dashed and solid lines are superimposed in this case. For ^{133}Cs case, relative variation reaches up to $\sim$ 75%.

the impact of the electric field on the strike pattern. Two key parameters are studied to determine the impact on the strike line: the perpendicular displacement of the strike line (perpendicular to the case without perturbation), $\delta_\perp$ in Fig. 6(a); and the modification of the intensity in the strike line due to the density and temperature perturbations in Fig. 6(b). Both species, ^{85,87}Rb and ^{133}Cs, available as separate sources in the AUG i-HIBP diagnostic, have been used in the analysis.

The relevant comparison in the strike line is the case without the electric field (solid lines) and with the electric field (dashed lines). For both species, the displacement caused only by the magnetic field perturbation lies in the range of $\sim 40\,\mu$m, while the electrostatic potential induces a deviation up to ~2 mm, above the expected optical resolution ($\sim 100\,\mu$m) on the scintillator. For the intensity pattern variation [Fig. 6(b)], the deviation due to the electric perturbation is negligible. The relative pattern variation is an order of magnitude difference between Cs and Rb beams, being $\approx$ 75% and $\approx$ 15%, respectively. This systematic deviation in intensity points to the possibility of measuring δn_e due to Alfvénic modes in the i-HIBP.

V. CONCLUSIONS

In this work, the synthetic diagnostics for fast-ion losses and the i-HIBP diagnostic have been developed and applied to a MEGA simulation. The synthetic fast-ion loss diagnostic shows already promising results, connecting the fast-ion losses to the interaction with Alfvénic phenomena, through E' lines. This methodology can now be extended to the rigorous study of plasma instabilities and understanding the fast-ion losses associated with them.

The preliminary study of the synthetic i-HIBP signal for the simulated AE shows that the radial structures may be resolved by the i-HIBP diagnostic. The impact on the strike line due to the electric

perturbation induced by the AEs will be measurable with the i-HIBP scintillator ($\approx$2 mm).

DATA AVAILABILITY

The data that support the findings of this study are available from the corresponding author upon reasonable request.

REFERENCES

[1] W. W. Heidbrink *et al.*, Nucl. Fusion **34**, 535–615 (1994).
[2] M. Shimada *et al.*, Nucl. Fusion **47**, S1 (2007).
[3] W. W. Heidbrink, Phys. Plasmas **15**, 055501 (2018).
[4] Y. Todo, Rev. Mod. Plasma Phys. **3**, 1 (2019).
[5] K.-L. Wong, Plasma Phys. Controlled Fusion **41**, R1 (1999).
[6] M. García-Muñoz *et al.*, Rev. Sci. Instrum. **80**, 053503 (2009).
[7] J. Gonzalez-Martin *et al.*, Rev. Sci. Instrum. **89**, 10I106 (2018).
[8] J. Gonzalez-Martin, in 22nd Energetic Particle Physics Topical Group Meeting of the ITPA, Ravaniemi, Finland, 2019.
[9] M. García-Muñoz *et al.*, Nucl. Fusion **50**, 084004 (2010).
[10] M. García-Muñoz *et al.*, Phys. Rev. Lett. **100**, 055005 (2008).
[11] M. García-Muñoz *et al.*, Phys. Rev. Lett. **104**, 185002 (2010).
[12] M. García-Muñoz *et al.*, Plasma Phys. Control. Fusion **61**, 054007 (2019).
[13] Y. Todo *et al.*, Phys. Plasmas **5**, 1321–1327 (1998).
[14] G. Birkenmeier *et al.*, J. Instrum. **14**, C10030 (2019).
[15] G. Anda *et al.*, Rev. Sci. Instrum. **89**, 013503 (2018).
[16] J. Galdon-Quiroga *et al.*, J. Instrum. **12**, C08023 (2017).
[17] Y. Todo *et al.*, Nucl. Fusion **56**, 112008 (2016).
[18] A. M. Dimits *et al.*, J. Comput. Phys. **107**, 309–323 (1993).
[19] J. Jacquinot *et al.*, Nucl. Fusion **39**, 2471–2494 (1999).
[20] J. Gonzalez-Martin, Ph.D. thesis, Universidad de Sevilla, 2021.
[21] J. P. Boris, in *Proceedings of the 4th Conference on Numerical Simulation of Plasmas* (Naval Research Laboratory, Washington D. C., 1970), pp. 3–67.
[22] W. Lotz, Astrophys. J., Suppl. Ser. **14**, 207 (1967).
[23] F. W. Meyer *et al.*, Phys. Lett. A **54**, 333–334 (1975).
[24] F. Ebel *et al.*, J. Phys. B: Atom. Mol. Phys. **20**, 4531–4542 (1987).
[25] R. J. Girnius *et al.*, Nucl. Instrum. Methods **143**, 505–511 (2002).
[26] E. Viezzer *et al.*, Plasma Phys. Controlled Fusion **53**, 035002 (2011).
[27] D. Wutte *et al.*, At. Data Nucl. Data Tables **65**, 155–180 (1997).
[28] F. Ryter *et al.*, Nucl. Fusion **53**, 113003 (2013).
[29] T. Möller *et al.*, J. Graphics Tools **2**, 21–28 (1997).
[30] D. R. Hertling *et al.*, J. Appl. Phys. **53**, 5427 (1982).
[31] M. J. Higgins *et al.*, Technical Report CLM-R294, Culham Laboratory, 1989.
[32] R. Jiménez-Gómez *et al.*, Nucl. Fusion **51**, 033001–033016 (2011).